electronics

MDPI

Article

Research on intelligent diagnosis model of keratoconus based on deep learning

Shulin Gao* †, Yvqian Yang†, Hao Zhou† and Yangrui Yang*

School of Information Engineering, North China University of Water Resources and Electric Power, Zhengzhou 450018, China

† These authors contributed equally to this work

* Correspondence: yangyangrui@ncwu.edu.cn(Y.Y.); 202018526@stu.ncwu.edu.cn(S.G.)

Abstract: In order to establish an intelligent diagnosis model of keratoconus by analyzing the characteristics of the patient 's keratoconus topographic map, in this study, various types of keratoconus topography maps obtained from the Ophthalmology Center of Henan Provincial People's Hospital were cleaned, cropped, normalized and standardized, and the Resnet50, Vision Transformer and CBAM-Resnet50 models were established. The above data were used to train the three models and test and analyze the optimal models of each network. Result shows that the CBAM-Resnet50 network model performed best. The accuracy, precision, recall, specificity, and F1-Score on the test set were 97.0 %, 98.0 %, 96.1 %, 98.0 %, and 97.0 %, respectively. The AUC value was 0.97. The accuracy is 10 % ~ 14 % higher than the other two models. Therefore, we conclude that CBAM-Resnet50 can be used for clinical high-precision keratoconus screening.

Keywords: Keratoconus; Keratoconus Topography; Deep Learning; Attention Mechanism; Image Classification

0. Introduction

Keratoconus is a primary corneal disease characterized by progressive thinning and anterior bulging of the central cornea, leading to corneal ectasia and a conical shape [1]. According to the research of Corneal Disease Group of the Chinese Society of Ophthalmology in 2019 [2], its incidence ranges from 5/10,000 to 23/10,000 worldwide. In advanced stages, keratoconus can significantly reduce visual acuity in a short period and treatment can be costly. Accordingly, early screening and treatment are crucial for preserving eye health. The pathogenesis of keratoconus remains unclear at present. Common diagnostic methods include corneal topography [3,23-26], Orbscan anterior segment analyzer [4], Pentacam anterior segment analyzer [5,27-31], anterior segment optical coherence tomography [6,32-33], and corneal biomechanical analyzer [7,34]. Corneal topography is a non-invasive technique that analyzes corneal morphology qualitatively and quantitatively and is widely used in keratoconus screening. However, traditional diagnostic methods are susceptible to environmental factors and subjective judgment by doctors, leading to potential misdiagnosis and low accuracy. Additionally, traditional screening methods can be time-consuming and inefficient when screening large populations. With the increasing demand for corneal laser surgery, accurately and rapidly screening for keratoconus has become an urgent clinical problem.

The birth of LeNet [8] in 1998 marked the official entry of image classification tasks into the era of deep learning. In this process, many convolutional neural networks with deeper layers and better performance were iteratively updated. However, deeper network structures often require larger computational resources and longer computation time, which is not tolerable in the screening process for keratoconus. Therefore, when attention mechanisms [9] and transfer learning emerged, keratoconus

Citation: To be added by editorial staff during production.

Academic Editor: Firstname Lastname

Received: date
Revised: date
Accepted: date
Published: date

screening theoretically became fast and accurate. Recently, Google modified the Transformer model to propose Vision Transformer for the field of computer vision. It completes image classification tasks by directly dividing images into several segments and combining them into a sequence as input. The team of Ao Dihua [12] once used Vision Transformer to classify keratoconus and obtained a Vision Transformer model with an accuracy rate of over 83% on a test set of 165 keratoconus topographic maps from 165 eyes. However, this method was achieved by selecting 7 types of original three-dimensional corneal topographic map data from Pentacam topographic maps. It requires standardizing various data in corneal topographic maps and then screening and extracting standardized data through mathematical analysis. The strong dependence on professional knowledge of keratoconus leads to extremely high complexity of this method.

Due to the high incidence of keratoconus and the serious consequences that may result in the late stage, existing screening methods for keratoconus can no longer meet practical needs. Although new technologies such as corneal topography have been widely used in preoperative keratoconus screening for corneal refractive surgery, there is still an urgent need for a simpler and more effective screening method to assist doctors in early detection and treatment of keratoconus patients. Based on this, this paper proposes a keratoconus screening method that can directly classify based on corneal topography. Combined with deep learning models, we established intelligent diagnostic models for keratoconus based on Resnet50, Vision Transformer and CBAM-Restnet50 and screened out the best model among the three established intelligent diagnostic models for keratoconus.

1 Data

This study used a total of 500 keratoconus topographic images from 500 patients who underwent keratoconus examination in the past two years at the Ophthalmology Center of Henan Provincial People's Hospital as experimental subjects. The data was divided into three parts: a training set of 300 cases with 300 eyes, a test set of 100 cases with 100 eyes, and a validation set of 100 cases with 100 eyes. Each type of data set contained 50% positive and negative samples. The data distribution table is shown in Table 1 below. The criteria for judging whether a patient has keratoconus are: (1) KISA index [13], whose calculation formula is:

$$KISA\% = \frac{(k) \times (I - S) \times (AST) \times (SRAX) \times 100}{300} \quad (1)$$

In the above formula, k represents the central corneal curvature (Keratometry), $I - S$ represents the difference between the steepest and flattest curvatures, $SRAX$ represents the relative offset of the steepest axis (Skewed Radial Axis), and AST represents the value of astigmatism. It is stipulated that a $KISA$ index greater than 100% indicates keratoconus and a $KISA$ coefficient less than 80% indicates normal cornea; (2) The difference in curvature between the largest and smallest circles of Placido rings. The standard value is set at $4.5D$. If it is greater than this value, it is judged to be keratoconus.

$$\begin{cases} a - b > 4.5D, \ keratoconus \\ a - b \leq 4.5D, \ normal\ cornea \end{cases} \quad (2)$$

In the above formula, a represents the curvature value of the largest circle of Placido rings and b represents the curvature value of the smallest circle of Placido rings. All patients involved in this study have signed informed consent forms and all data processes comply with the requirements of the Helsinki Declaration.

Table 1. Dataset distribution table

Data Set	Number of eyes (Eyes)	normal cornea (Eyes)	Keratoconus (Eyes)
Training set	300	150	150
Test set	100	50	50
Validation set	100	50	50

2. Method

In this study, medical images were first denoised and cleaned before being loaded into a data loader with appropriate transformations. Three deep neural networks were established and trained using the training set to obtain Resnet50, Vision Transformer, and CBAM-Resnet50 classifiers. The model was tuned using the validation set and grid search was used for parameter iteration. After adjusting the training settings and setting the training parameters, the model was trained. Finally, the performance of the model on the test set was evaluated and the best performing model was selected as the final keratoconus intelligent diagnosis model. The algorithm flowchart of this study is shown in Figure 1.

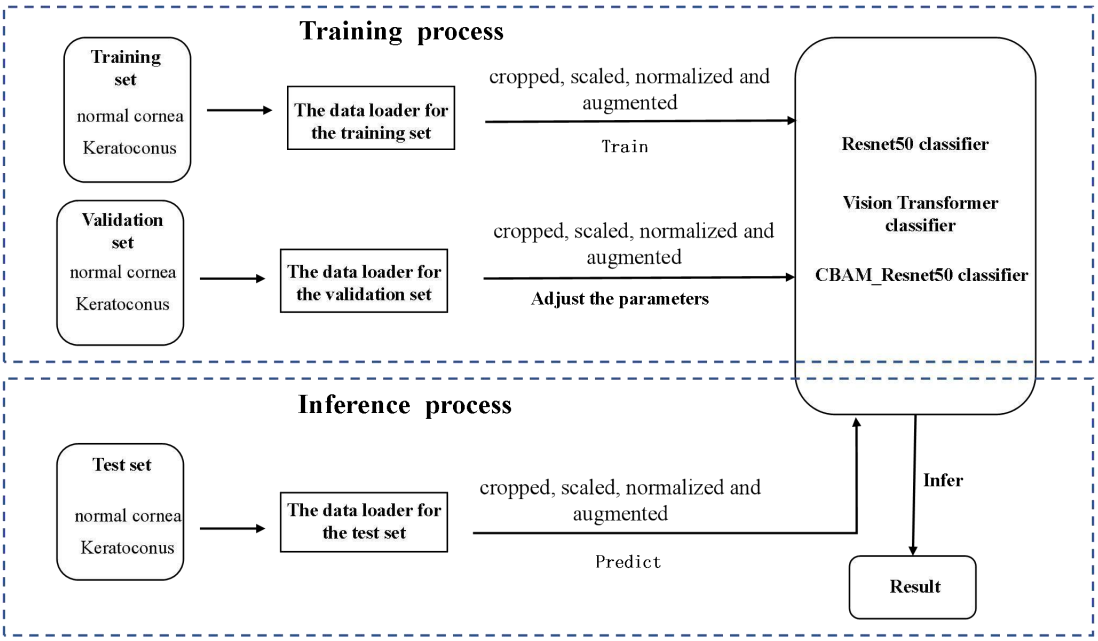

Figure 1. Algorithm flowchart of this article

2.1 Data processing

The classified data needs to be further processed on the images. This process mainly involves removing excess markings and irrelevant information from the original keratoconus topography maps. The processed images consist of a total of 4 images per

case per eye, distributed in the four corners of the image. The images before and after removing irrelevant information are shown in Figure 2.

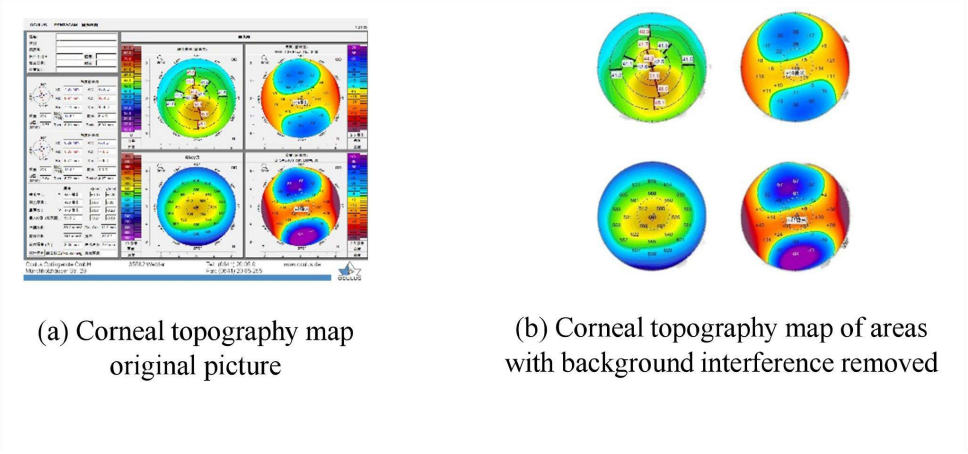

(a) Corneal topography map original picture

(b) Corneal topography map of areas with background interference removed

Figure 2. Original map(a) and topographic map(b) of keratoconus after cleaning

After denoising the data, 500 RGB three-channel images with a size of 686×686 were obtained. The training set, test set and validation set were cropped, scaled, normalized and augmented using the torchvision tool and converted to tensor type.

2.2 Modeling

Resnet50 model: The Fine Tuning transfer learning algorithm [14] is used to retain the parameters of the Resnet50 [15] network trained on the imagenet [20] dataset to initialize the network. The mapping dimension of the fully connected layer on the target network is adjusted, that is, two dimensions of keratoconus and normal cornea. Finally, the confidence level belonging to both is obtained.

$$\text{result} = \max(p, q) \tag{3}$$

Where p represents the confidence level that the model predicts as keratoconus and q represents the confidence level that the model predicts as normal cornea. The advantage of doing this is that by using data on large models to initialize the model, fine-tuning can be in a better position, thereby making the network converge faster. The reason for choosing the Resnet50 network is that it has a residual structure [15], that is, a residual block. Its structural diagram is shown in Figure 3.

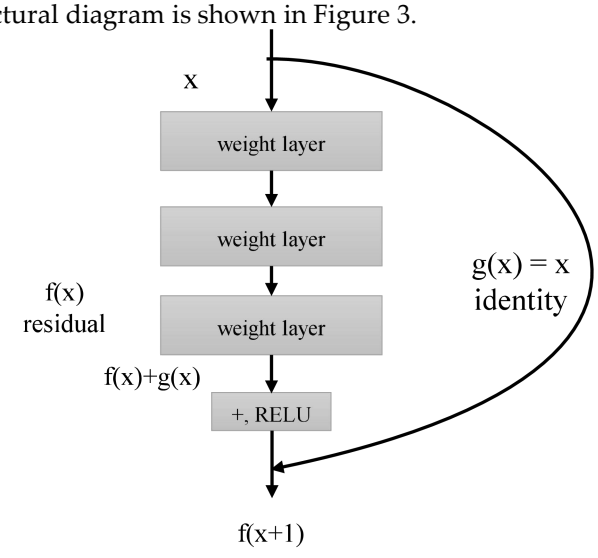

Figure 3. Schematic diagram of the residual block

Its expression is:

$$f(x+1) = \sigma(f(x) + g(x)) \tag{4}$$

In the above formula, σ represents the Relu activation operation. f(x) represents the feature map obtained by directly inputting x into the residual block. g(x) represents x after an identity mapping [21]. $f(x)$ represents x after a residual mapping. The output of identity mapping is equal to the input, that is, $g(x) = x$. Let x_l and x_L represent the input and output of the residual unit, and F be the learned residual. The feature learned in the accumulated residual blocks is:

$$x_L = x_l + \sum_{i=l}^{L-l} F(x_i, W_i) \tag{5}$$

When the model is learned well enough, $x_L = 0$ and the network degrades into a shallow network with high accuracy. The complete Resnet50 network in this study is shown in Figure 4.

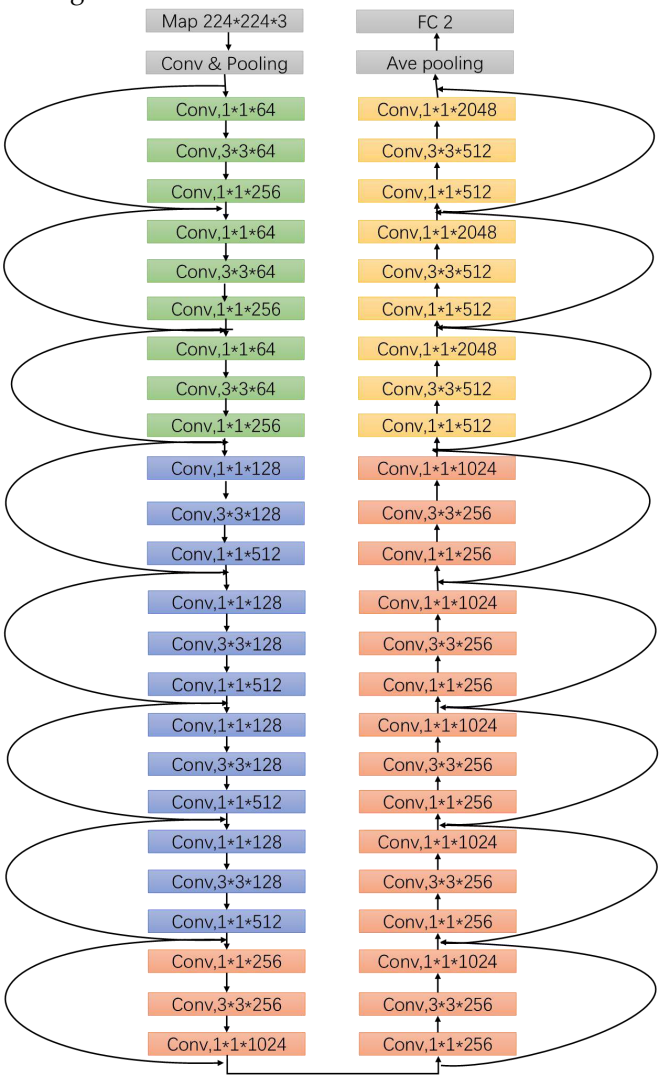

Figure 4. Residence diagram of the resnet50 network in this paper

Vision Transformer model： A model is established using the Vision Transformer network [10,11]. The keratoconus topography map is divided into several 16×16 local images and spliced into a sequence and encoded as:

$$A = (x_1, x_2, x_3, x_4, x_5, \ldots\ldots x_n) \tag{6}$$

After the following linear transformation, a vector B containing the content information of the image is obtained:

$$y_i = Wx_i + b \tag{7}$$

$$B = (Wx_1 + b, Wx_2 + b, Wx_3 + b, Wx_4 + b, Wx_5 + b \ldots\ldots Wx_n + b) \tag{8}$$

In this process, W and b are parameters of the linear transformation and are shared among all vectors. The vector sequence is then positionally encoded and a new vector z_0 representing the category is added to the head of the sequence to form a new vector sequence C.

$$C = (z_0, z_1, z_2, z_3, z_4, z_5 \ldots\ldots z_n) \tag{9}$$

Sequence C is fed into the network and a classification model is obtained using the network's encoder-decoder structure and multi-head attention mechanism. The specific structure of the multi-head attention mechanism is shown in Figure 5.

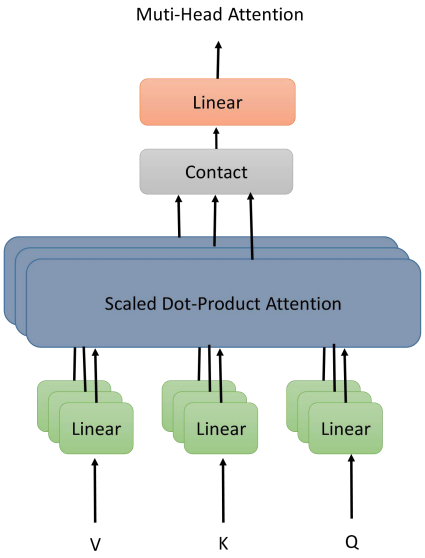

Figure 5. Diagram of the Muti-Head Attention

In the multi-head attention mechanism, the sequence C is transformed linearly to obtain vectors Q (Query), K (Key), and V (Value), where:

$$Q = W_1 C \tag{10}$$

$$K = W_2 C \tag{11}$$

$$V = W_3 C \tag{12}$$

In the above formula: $W_1 \neq W_2 \neq W_3$. Q is used to calculate the relationship vector between the current position and other positions. K is used to match with the Q vector. V is multiplied by the matched Q vector and its value represents the output at that position, representing the distance relationship between Q and the currently matched value. The values of W_1, W_2 and W_3 are iteratively updated through a loss function. Compared with traditional neural networks, this model directly uses encoding and decoding operations to classify corneal cones without using convolution operations.

Its main kernel is a multi-head attention mechanism. The structure of the model is shown in Figure 6 below.

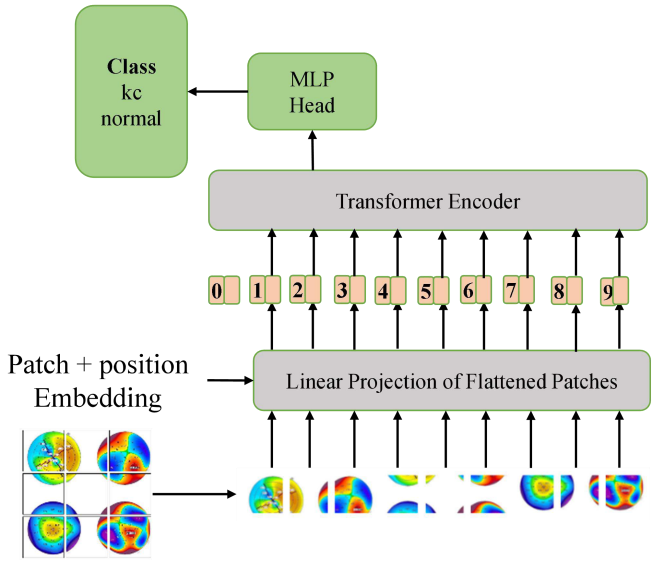

Figure 6. Diagram of the Vision Transformer network in this paper

CBAM-Resnet50 model： A model is built using the attention mechanism. The attention mechanism is divided into channel attention mechanism and spatial attention mechanism. This paper uses a combination of the two, CBAM model [16], to focus on some important features of the feature map. CBAM includes two sub-modules: CAM (Channel Attentional Module) and SAM (Space Attentional Module), which perform attention in the channel and spatial dimensions respectively. CAM and SAM jointly recalibrate the feature map to emphasize informative features and suppress useless features, thereby improving the performance of CNNs. The additional overhead generated by CBAM can be ignored, so it can be integrated into any CNN architecture. According to CBAM [16], processing images with CAM module before SAM module is conducive to improving the accuracy of model prediction. This is because using channel attention mechanism first can better focus on features in images and improve the robustness of the model. Therefore, this paper's CBAM-Resnet50 model mainly implements by adding a CBAM attention mechanism model after each residual block in Resnet50 backbone network. The structure diagram of CBAM is shown in Figure 7 below.

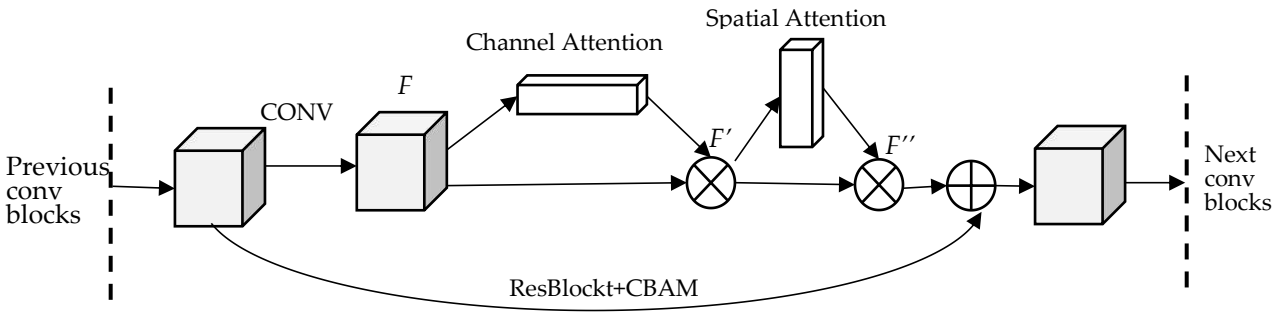

agram of the CBAM

For an input feature map F with size H×W×C, CBAM will infer a channel attention map Mc with size C×1×1 in the channel attention mechanism and a spatial attention map Ms with size 1×H×W in the spatial attention mechanism.

$$F' = M_c(F) \otimes F \tag{13}$$

$$F'' = M_s(F') \otimes F' \tag{14}$$

In the channel attention module, after the features undergo global max pooling and global average pooling based on width and height, they are processed by a multi-layer perceptron (MLP) and then added together to form a tensor. The sigmoid function is then used for activation to generate the final channel attention map Mc as follows:

$$M_c(F) = \sigma(MLP(AvgPool(F)) + MLP(MaxPool(F))) \tag{15}$$

In the spatial attention mechanism, after the features undergo global max pooling and global average pooling based on channels, the two resulting feature maps are combined into a feature map Ms with 2 channels as follows:

$$M_s(F) = \sigma(f^{7\times7}(A[vgPool(F)\ ;\ MaxPool(F)])) \tag{16}$$

The extracted feature map is mapped to two dimensions, corresponding to normal cornea and conical cornea. The CBAM-RESNET50 model in this paper is shown in Figure 8 below.

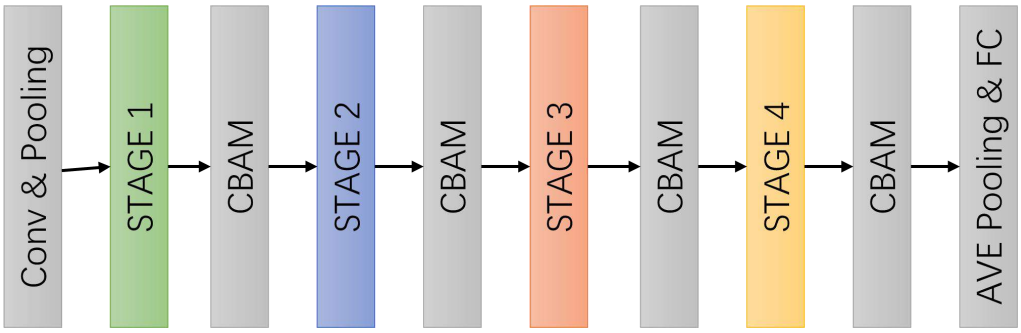

Figure 8. Diagram of the CBAM-Restnet50 network in this paper

2.3 Training Settings

After the model is built, the conical cornea dataset is preprocessed, including operations such as cropping, data augmentation, normalization and data tensorization. The data is trained through the above Resnet50, Vision Transformer and CBAM-RESNET50 models and compared experimentally. During training, the training set: test set: validation set = 3:1:1. The Adam optimizer is selected to implement gradient descent optimization and cross-entropy loss function is used for backpropagation of the model. The results are validated using validation set data and parameters are adjusted accordingly. Every 20 rounds, the learning rate is reduced by 0.05 to better fit the model. The number of training rounds is set to 300 and the model with the highest accuracy on the test set during training is selected as the final conical cornea classification model. During training, it is necessary to record in real time the evaluation parameters of each round of the model. Evaluation parameters include confusion matrix, precision rate, recall rate, F1 Score, ROC curve and AUC value.

3. Results

3.1 Numerical Results

Through training of the above three networks, the best models under the corresponding networks are finally obtained. The confusion matrices of these models on the test set are shown in Figure 9 below.

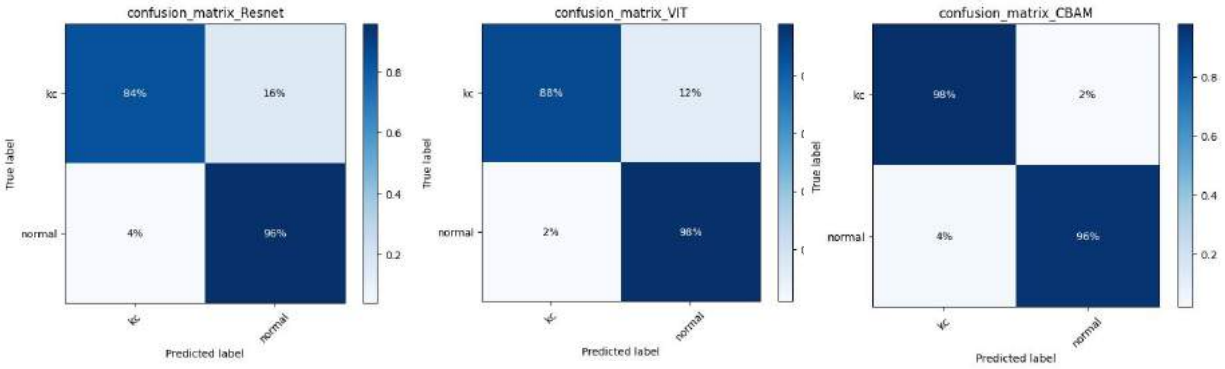

(a) Confusion matrix of Resnet50 (b) Confusion matrix of Vision Transformer (c) Confusion matrix of CBAM-Resnet50

Figure 9. Confusion matrices of three models on the test set. Part (a) is the Confusion matric of Resnet50. Part (b) is the Confusion matric of Vision Transformer. Part (c) is the Confusion matrices of CBAM-Resnet50.

From Figure 9 above, it can be seen that through the confusion matrices of the three models mentioned above and then through Formulas as follows, the accuracy, precision, recall rate, specificity and F1 Score of the three models are obtained and the results are shown in Table 2.

$$Accuracy:\ ACC = \frac{TP+TN}{TP+TN+FP+FN} \tag{17}$$

$$Precision:\ PPV = \frac{TP}{TP+FP} \tag{18}$$

$$Recall:\ REC = \frac{TP}{TP+FN} \tag{19}$$

$$Specificity:\ TNR = \frac{TN}{TN+FP} \tag{20}$$

$$F1\text{-}Score:\ F1 = \frac{2\times TP}{2\times TP+FN+FP} \tag{21}$$

In the above formula, TP represents the number of cases where the true value is keratoconus and the model considers it to be keratoconus; TN represents the number of cases where the true value is keratoconus and the model considers it to be a normal cornea. This value represents the number of keratoconus samples that have a statistical Type I error in this model. FP represents the number of cases where the true value is a normal cornea and the model considers it to be keratoconus. This value represents the number of keratoconus samples that have a statistical Type II error in this model. FN represents the number of cases where the true value is a normal cornea and the model considers it to be a normal cornea.

Table 2. Secondary indicators of the three models

Model Name	ACC	PPV	REC	TNR	F1-Score

Resnet50	90.0%	84.0%	95.5%	85.7%	89.4%
Vision Transformer	93.0%	88.0%	97.8%	89.1%	92.6%
CBAM-Resnet50	97.0%	98.0%	96.1%	98.0%	97.0%

From the data in Table 2, it can be clearly seen that the accuracy, precision, recall rate, specificity and F1-Score of Resnet50 are 90.0%, 84.0%, 95.5%, 85.7% and 89.4% respectively; the accuracy, precision, recall rate, specificity and F1-Score of Vision Transformer are 93.0%, 88.0%, 97.8%, 89.1% and 92.6% respectively; the accuracy, precision, recall rate, specificity and F1-Score of CBAM-RESNET50 are 97.0%, 98.0%, 96.1%, 98.0% and 97.0% respectively. Compared to Resnet50, Vision Transformer has an overall increase of 3.3% in accuracy, an overall increase of 4.7% in precision rate and an overall increase of about 3.9% in specificity. Compared to Vision Transformer CBAM-RESNET50 has an overall increase of about 11.36% in precision rate and an overall increase of about 4.0% in F1-Score value but their recall rates are not much different and both above 96.0%. Comparing these three models with the five indicators used to measure them CBAM-RESNET50 has the highest accuracy which means it can make the most precise judgment on a given keratoconus topographic map while its high precision reflects that when given a keratoconus topographic map this model has only a probability of making a mistake at about 0.03. Additionally, this model has a high recall rate which means it is strong at screening for keratoconus topographic maps being able to screen out more target samples from the same test data (100 positive and negative samples). Although its recall rate is lower than that of VIT model its precision and sensitivity are much higher than those of VIT model indicating that this model is most sensitive for keratoconus topography examination tasks with highest accuracy thus having greatest application value. Therefore, from all these indicators it can be concluded that CBAM-RESNET50 is the best performing model.

3.2 Curve Results

In terms of curve results this study chose the ROC curve as the main indicator to reflect the quality of the model. The ROC curve can better and more easily find out the recognition ability of the model at any threshold value. Generally speaking, the more convex and closer to the upper left corner an ROC curve is the greater value it has for diagnosing keratoconus. The ROC curve of the model on test set obtained through testing is shown in Figure 10 below.

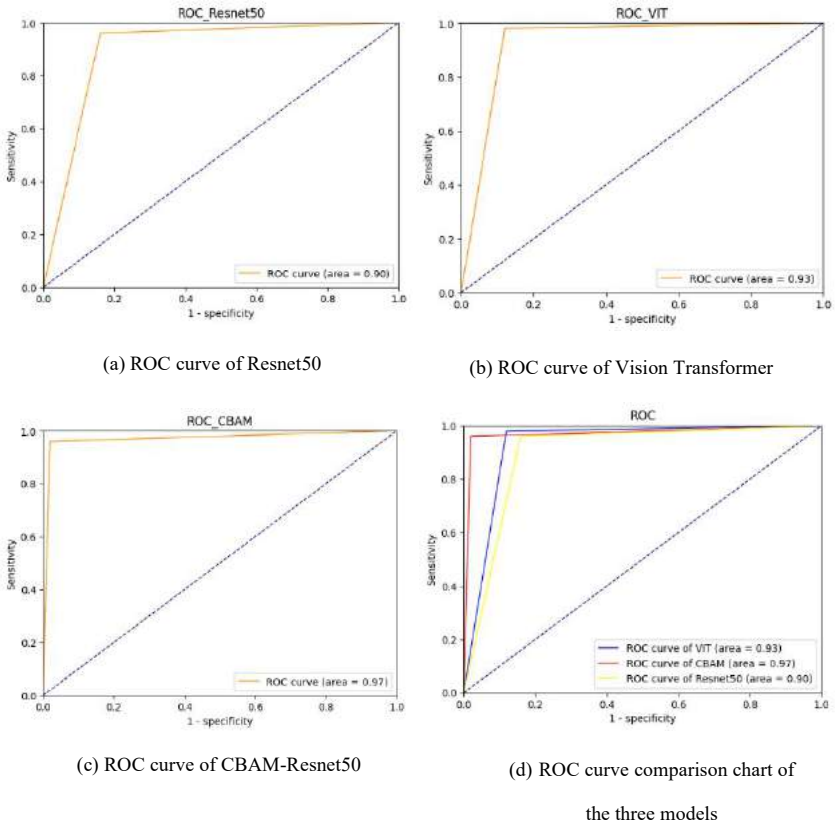

(a) ROC curve of Resnet50

(b) ROC curve of Vision Transformer

(c) ROC curve of CBAM-Resnet50

(d) ROC curve comparison chart of the three models

Figure 10. ROC plots of the three models

In the curve graphs of Figure 3 (a), (b) and (c) the AUC values of Resnet50 Vision Transformer and CBAM-RESNET50 are 0.90 0.93 and 0.97 respectively. The value of AUC can roughly reflect the left convexity of the ROC curve. Generally speaking, the more convex to the left an ROC curve is the larger its AUC value is and the better its corresponding model is. In (d) CBAM-RESNET50's curve is on the far left with its corresponding AUC value being the largest indicating that CBAM-RESNET50 has the best performance among these three models.

3.3 Interpretability Analysis

The above experimental results show that among the three models defined in this paper CBAM-Resnet50 has the best effect in diagnosing whether a patient has keratoconus using keratoconus topographic maps with an accuracy rate of up to 97%. According to class activation mapping [22] visualizing randomly selected keratoconus topographic map test samples using heat maps produces images like Figure 11 below.

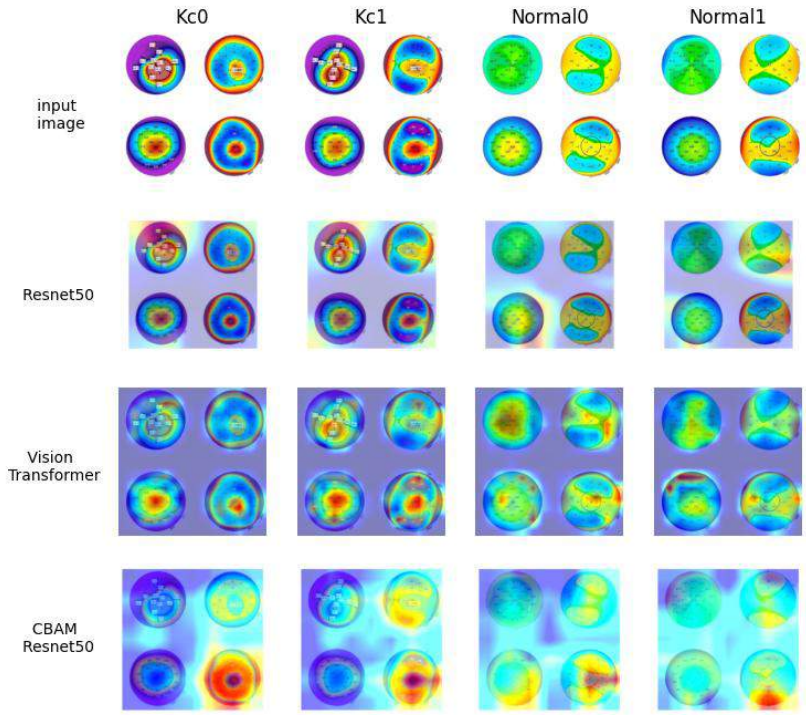

Figure 11. Interpretable analysis heatmaps for Resnet50, Vision Transformer, CBAM-Resnet50

Figure 11 shows the interpretability heat maps of Restnet50 network VIT network and CBAM-RESNET50 network. The parts with reddish color are the parts that the model pays special attention to during learning while the parts with bluish color are not particularly focused on by the model during learning. It can be seen that due to different networks used the local features that models pay attention to during learning also differ. Using residual networks models pay more attention to the edges of images in order to judge whether it is keratoconus. Similarly using residual networks after introducing CBAM-RESNET50 network the area that models pay attention to is significantly increased compared to when CBAM-RESNET50 network was not introduced and models value previously important features more than when CBAM-RESNET50 network was not introduced. VIT model uses Transformer network structure and when inputting into the network it inputs a sequence of a keratoconus topographic map divided into 16×16 local maps and stretched to one dimension. The model learns more about corneal features during learning which is actually consistent with doctors' diagnostic basis in practice. Therefore overall under the premise of sufficient data VIT model performs better than CBAM-RESNET50 and Resnet network introducing CBAM-RESNET50 performs better than same one without introducing CBAM-RESNET50 but due to confidentiality of medical image data this paper has limited data so VIT model performs slightly weaker than CBAM-RESNET50.

4. Discussion

At present the international treatment plan for keratoconus is early detection and intervention of lesions and timely treatment. However, the clinical diagnosis methods for keratoconus are not perfect and most require doctors to have rich medical experience and theoretical experience especially since the clinical manifestations of early keratoconus are not obvious which greatly increases the workload of relevant ophthalmologists. Although Pentacam tomography technology can analyze data such as anterior and posterior corneal contours and heights thickness astigmatism pupil size anterior chamber depth 3D model of anterior segment etc. to play a certain auxiliary role

in the diagnosis of keratoconus with the increasing demand for corneal laser surgery in recent years how to accurately and quickly screen for keratoconus is a problem that needs to be solved urgently in clinical practice. Artificial intelligence algorithms have the advantages of continuous learning and iterative updating. They can systematically learn from previous patients' keratoconus topographic maps extract their features analyze important and unimportant features classify patients' corneas into two categories quickly and accurately discover whether corneal lesions have occurred.

In previous studies most researchers used corneal topographic maps output by Pentacam tomography technology extracted several most sensitive standardized parameters among various standardized parameters for judging whether a cornea is a keratoconus task performed data analysis selected the most suitable parameters into machine learning models to achieve diagnosis of keratoconus; Cao et al. [17] screened out 5 standardized parameters with the highest sensitivity into machine learning models for training finally obtained a random forest model with an accuracy rate of 98%; Chen et al. [18] screened out axial maps anterior-posterior elevation maps and thickness measurement maps into machine learning models for training finally obtained a CNN model with an accuracy rate of 97.85%; Shen et al. [19] selected 10 standardized parameters into machine learning models for training. Although using mathematical analysis to select standardized parameters with high correlation to train keratoconus classifiers has been practiced there is generally subjective misjudgment when selecting standardized parameters. When this error is included in machine learning models it often causes the effect of the model to shift in one direction. If a method is proposed that allows machines to select features through learning then choose which part (parameter) or parts (parameters) they focus on by themselves it can avoid this problem to some extent.

This paper constructs three deep learning network models namely Resnet50 network Vision Transformer network and CBAM-RESNET50 network selects 300 cases of 300 eyes completely annotated keratoconus topographic maps as input to the network finally obtains three models respectively. As described earlier CBAM-RESNET50 uses a combination of channel attention mechanism and spatial attention mechanism so that during recognition some parts that determine whether it is keratoconus (such as central heart of corneal image) increase weight while some unimportant parts (such as edge part of corneal image) reduce weight appropriately. This mechanism allows model to perform targeted calculations on various parts during recognition process which significantly outperforms Resnet50 model without introducing CBAM network when data volume is small VIT model can be used for high-precision screening work on clinical keratoconus. The results are only reference results for diagnosis in actual application doctors need diagnose based on patient's own situation. In near future enrich relevant data refine algorithm improve medical facilities realize intelligent collection analysis all data related patient's cornea enhance robustness precision screening.

References

1. SUI Yao,XING Jiannan,ZHAO Haixia. Diagnosis and treatment of the status quo and new development of keratoconus.*China Medical Herald*,2016(29):32-36. [CrossRef]
2. Corneal Disease Group, Ophthalmology Branch of Chinese Medical Association. Chinese expert consensus on keratoconus diagnosis and treatment (2019)[J].*Chinese Journal of Ophthalmology*,2019,55(12):891-895. [CrossRef]
3. Cavas-Martínez, F., De la Cruz Sánchez, E., Nieto Martínez, J., Fernández Cañavate, F. J., & Fernández-Pacheco, D. G. (2016). Corneal topography in keratoconus: state of the art. *Eye and vision*, 3, 1-12. [CrossRef]
4. Amiri, M. A., Hashemi, H., Ramin, S., Yekta, A., Taheri, A., Nabovati, P., & Khabazkhoob, M. (2017). Corneal thickness

measurements with Scheimpflug and slit scanning imaging techniques in keratoconus. *Journal of Current Ophthalmology*, 29(1), 23-27. [CrossRef]

5. LUO Yi, HOU Xiaoyan, LI Wei. Clinical application of Pentacam anterior segment analyzer in the diagnosis of early keratoconus[J].*International Journal of Ophthalmology*,2020,20(9):1603-1606. [CrossRef]
6. WANG Chunxiao. Application of anterior segment optical coherence tomography in the diagnosis and treatment of corneal diseases[D]. Guangdong:Sun Yat-sen University,2010.[CrossRef]
7. CHEN Xinyan,QIN Xiao,ZHANG Haixia,LI Lin. Application of visualization corneal biomechanics analyzer in ophthalmology[J].*China Medical Equipment*,2018,33(7):101-106.[CrossRef]
8. LeCun, Y., Bottou, L., Bengio, Y., & Haffner, P. (1998). Gradient-based learning applied to document recognition. *Proceedings of the IEEE*, 86(11), 2278-2324.[CrossRef]
9. Vaswani, A., Shazeer, N., Parmar, N., Uszkoreit, J., Jones, L., Gomez, A. N., ... & Polosukhin, I. (2017). Attention is all you need. *Advances in neural information processing systems*, 30.[CrossRef]
10. Chen, L., Zhao, Y., & Li, X. (2022, November). Transformer terminal feature recognition and positioning method based on binocular vision and image processing algorithm. *In Second International Conference on Optics and Communication Technology* (ICOCT 2022) (Vol. 12473, pp. 383-393). SPIE.[CrossRef]
11. He, Z. (2022, March). The Application of Vision Transformer in Image Classification. *In Proceedings of the 6th International Conference on Virtual and Augmented Reality Simulations* (pp. 56-63).[CrossRef]
12. Ao Dihua, Tian Xirui, Ma Mingxun, Zhang Bo, Chen Min, Peng Yanli. Research on intelligent diagnosis model of keratoconus based on machine deep learning algorithm[J].*International Journal of Ophthalmology*,2023,23(2):299-304.[CrossRef]
13. Rabinowitz, Y. S., & Rasheed, K. (1999). KISA% index: a quantitative videokeratography algorithm embodying minimal topographic criteria for diagnosing keratoconus. *Journal of Cataract & Refractive Surgery*, 25(10), 1327-1335.[CrossRef]
14. Xie, M., Jean, N., Burke, M., Lobell, D., & Ermon, S. (2016, March). Transfer learning from deep features for remote sensing and poverty mapping. *In Proceedings of the AAAI conference on artificial intelligence* (Vol. 30, No. 1).[CrossRef]
15. He, K., Zhang, X., Ren, S., & Sun, J. (2016). Deep residual learning for image recognition. *In Proceedings of the IEEE conference on computer vision and pattern recognition* (pp. 770-778).[CrossRef]
16. Woo, S., Park, J., Lee, J. Y., & Kweon, I. S. (2018). Cbam: Convolutional block attention module. *In Proceedings of the European conference on computer vision* (ECCV) (pp. 3-19).[CrossRef]
17. Cao, K., Verspoor, K., Chan, E., Daniell, M., Sahebjada, S., & Baird, P. N. (2021). Machine learning with a reduced dimensionality representation of comprehensive Pentacam tomography parameters to identify subclinical keratoconus. *Computers in Biology and Medicine,* 138, 104884.[CrossRef]
18. Chen, X., Zhao, J., Iselin, K. C., Borroni, D., Romano, D., Gokul, A., ... & Zheng, Y. (2021). Keratoconus detection of changes using deep learning of colour-coded maps. *BMJ Open Ophthalmology*, 6(1), e000824.[CrossRef]
19. Shen, Y., Xian, Y., Han, T., Wang, X., & Zhou, X. (2021). Bilateral Differential Topography—A Novel Topographic Algorithm for Keratoconus and Ectatic Disease Screening. *Frontiers in Bioengineering and Biotechnology*, 1162.[CrossRef]
20. Deng, J., Dong, W., Socher, R., Li, L. J., Li, K., & Fei-Fei, L. (2009, June). Imagenet: A large-scale hierarchical image database. *In 2009 IEEE conference on computer vision and pattern recognition* (pp. 248-255). Ieee.[CrossRef]
21. He, K., Zhang, X., Ren, S., & Sun, J. (2016). Identity mappings in deep residual networks. *In Computer Vision–ECCV 2016: 14th European Conference, Amsterdam, The Netherlands, October 11–14, 2016, Proceedings*, Part IV 14 (pp. 630-645). Springer International Publishing.[CrossRef]
22. Zhou, B., Khosla, A., Lapedriza, A., Oliva, A., & Torralba, A. (2016). Learning deep features for discriminative localization. *In Proceedings of the IEEE conference on computer vision and pattern recognition* (pp. 2921-2929).[CrossRef]
23. Mei Ying, Tang Zhiping. Study on the efficiency of keratotopographic mapping software simulation function fitting

keratoconus contact lens[J].*Traffic Medicine*,2020,34(5):522-524.[CrossRef]

24. ZHANG Xiaofeng,LI Longbiao,ZHANG Jiming. Screening of keratoconus in myopic eyes[J].*Chinese Journal of Practical Ophthalmology*,2002,20(3):191-193.[CrossRef]
25. HE Bihua, ZHANG Li, TAO Ping, CHEN Ping, ZHOU Y, YANG Bo, & XIE Hao. (2019). Corneal topographic map morphological features and early diagnosis of keratoconus. *Modern Instruments & Medical*.[CrossRef]
26. Xiao Ming, Ma Daijin. Combined application of Corvis ST and Pentacam corneal topography for the diagnosis of keratoconus[J].*Ophthalmology*,2019,28(2):150-154.[CrossRef]
27. XU Miao, XU Yingnan, XUE Jinsong. Clinical study on diagnosis of early keratoconus based on morphological parameters of ocular surface with different corneal diameters[J].*International Journal of Ophthalmology*,2023,23(2):267-272.[CrossRef]
28. LI Feng, ZHAO Zhihui, CHEN Shuang, WU Xiaolei. Pentacam anterior segment analysis system to study the relationship between astigmatism and keratoconus[J].*International Journal of Ophthalmology*,2022,22(4):669-672.[CrossRef]
29. WANG Huiyu,ZHAO Shaozhen,HE Meinan,DU Bei,DONG Xiaojun. Diagnostic value of anterior segment analyzer examination parameters in early keratoconus[J].*International Journal of Ophthalmology*,2021,21(10):1812-1815.[CrossRef]
30. WU Yongjuan, LI Zuwei, HE Zufeng. Differential diagnostic value of Pentacam anterior segment analyzer for highly myopic astigmatism and subclinical keratoconus[J].*Chinese Journal of Modern Medicine*,2021,23(6):19-23.[CrossRef]
31. LUO Yi, HOU Xiaoyan, LI Wei. Clinical application of Pentacam anterior segment analyzer in the diagnosis of early keratoconus[J].*International Journal of Ophthalmology*,2020,20(9):1603-1606.[CrossRef]
32. LI Caihong, ZHAO Hong, JIA Bo, MA Shiji, GUO Huijuan. Safety and efficacy of rapid corneal collagen cross-linking in the treatment of keratoconus[J].*New Advances in Ophthalmology*,2020,40(3):243-246.[CrossRef]
33. Bi Yanlong, Chen Ranran, Sui Guiqin, Liu Zhenxing, Liu Xin, Niu Yunli, Wang Zhen, Zhou Qi. Treatment of acute keratoconus edema by deep lamellar keratoplasty with the same implant after corneal surface lens surgery[J].*Chinese Journal of Ocular Trauma and Occupational Ophthalmology*,2016,38(1):6-10.[CrossRef]
34. LIU Guoying,JING Lili,LI Jie,DU Xianli. The value of corneal stress-strain index in keratoconus diagnosis and the change of corneal biomechanical parameters after CXL surgery[J].*Chinese Journal of Ophthalmology*,2022,58(8):584-591.[CrossRef]
35. Qin Yu (review), Liang Gang (revised). Application of Corvis-ST corneal biomechanical measurement in corneal refractive surgery[J].*Hainan Medical Journal*,2022,33(7):943-946.[CrossRef]